Mid-infrared supercontinuum generation to 12.5m in large NA chalcogenide step-index fibres pumped at 4.5m

Kubat, Irnis; Agger, Christian; Møller, Uffe Visbech; Seddon, Angela B.; Tang, Zhuoqi; Sujecki, Slawomir; Benson, Trevor M.; Furniss, David; Lamrini, Samir; Scholle, Karsten

Total number of authors:
16

Published in:
Optics Express

Link to article, DOI:
10.1364/OE.22.019169

Publication date:
2014

Document Version
Publisher's PDF, also known as Version of record

Mid-infrared supercontinuum generation to 12.5μm in large NA chalcogenide step-index fibres pumped at 4.5μm

Irnis Kubat,[1,*] **Christian S. Agger,**[1] **Uffe Møller,**[1] **Angela B. Seddon,**[2] **Zhuoqi Tang,**[2] **Slawomir Sujecki,**[2] **Trevor M. Benson,**[2] **David Furniss,**[2] **Samir Lamrini,**[3] **Karsten Scholle,**[3] **Peter Fuhrberg,**[3] **Bruce Napier,**[4] **Mark Farries,**[5] **Jon Ward,**[6] **Peter M. Moselund,**[7] **and Ole Bang**[1,7]

[1]*DTU Fotonik, Department of Photonics Engineering, Technical University of Denmark, 2800 Kgs. Lyngby, Denmark*
[2]*George Green Institute for Electromagnetics Research, Faculty of Engineering, University Park, University of Nottingham, Nottingham NG7 2RD, UK*
[3]*LISA Laser Products OHG, Fuhrberg & Teichmann Max-Planck-Str. 1, 37191 Katlenburg-Lindau Germany*
[4]*Vivid Components Ltd., Dr.-Rörig-Damm 22, 33102 Paderborn, Germany*
[5]*Gooch & Housego (Torquay) Ltd., Broomhill Way, Torquay, Devon, TQ2 7QL, UK*
[6]*Gooch & Housego (UK) Ltd., Dowlish Ford, Ilminster, Somerset, TA19 OPF, UK*
[7]*NKT Photonics A/S, Blokken 84, 3460 Birkerød, Denmark*
[*]*ikub@fotonik.dtu.dk*

Abstract: We present numerical modeling of mid-infrared (MIR) supercontinuum generation (SCG) in dispersion-optimized chalcogenide (CHALC) step-index fibres (SIFs) with exceptionally high numerical aperture (NA) around one, pumped with mode-locked praseodymium-doped (Pr^{3+}) chalcogenide fibre lasers. The 4.5um laser is assumed to have a repetition rate of 4MHz with 50ps long pulses having a peak power of 4.7kW. A thorough fibre design optimisation was conducted using measured material dispersion (As-Se/Ge-As-Se) and measured fibre loss obtained in fabricated fibre of the same materials. The loss was below 2.5dB/m in the 3.3-9.4μm region. Fibres with 8 and 10μm core diameters generated an SC out to 12.5 and 10.7μm in less than 2m of fibre when pumped with 0.75 and 1kW, respectively. Larger core fibres with 20μm core diameters for potential higher power handling generated an SC out to 10.6μm for the highest NA considered but required pumping at 4.7kW as well as up to 3m of fibre to compensate for the lower nonlinearities. The amount of power converted into the 8-10μm band was 7.5 and 8.8mW for the 8 and 10μm fibres, respectively. For the 20μm core fibres up to 46mW was converted.

OCIS codes: (060.2390) Fiber optics, infrared; (190.4370) Nonlinear optics, fibers; (160.2750) Glass and other amorphous materials.

References and links

1. S. Dupont, C. Petersen, J. Thøgersen, C. Agger, O. Bang, and S. R. Keiding, "IR microscopy utilizing intense supercontinuum light source," Opt. Express **20**, 4887–4892 (2012).

#213711 - $15.00 USD Received 9 Jun 2014; revised 18 Jul 2014; accepted 19 Jul 2014; published 31 Jul 2014

2. C. A. Michaels, T. Masiello, and P. M. Chu, "Fourier transform spectrometry with a near-infrared supercontinuum source," Appl. Spectrosc. **63**, 538–543 (2009).
3. M. Kumar, M. N. Islam, F. L. Terry, M. J. Freeman, A. Chan, M. Neelakandan, and T. Manzur, "Stand-off detection of solid targets with diffuse reflection spectroscopy using a high-power mid-infrared supercontinuum source," Appl. Opt. **51**, 2794–2807 (2012).
4. C. Xia, M. Kumar, M.-Y. Cheng, R. S. Hegde, M. N. Islam, A. Galvanauskas, H. G. Winful, F. L. Terry, M. J. Freeman, M. Poulain, and G. Mazé, "Power scalable mid-infrared supercontinuum generation in ZBLAN fluoride fibers with up to 1.3 watts time-averaged power," Opt. Express **15**, 865–871 (2007).
5. C. Xia, Z. Xu, M. Islam, F. L. Terry, M. Freeman, A. Zakel, and J. Mauricio, "10.5 W time-averaged power mid-IR supercontinuum generation extending beyond 4μm with direct pulse pattern modulation," IEEE J. Sel. Top. Quantum Electron. **15**, 422–434 (2009).
6. G. Qin, X. Yan, C. Kito, M. Liao, C. Chaudhari, T. Suzuki, and Y. Ohishi, "Supercontinuum generation spanning over three octaves from UV to 3.85 μm in a fluoride fiber," Opt. Lett. **34**, 2015–2017 (2009).
7. P. M. Moselund, C. Petersen, S. Dupont, C. Agger, O. Bang, and S. R. Keiding, "Supercontinuum - broad as a lamp bright as a laser, now in the mid-infrared," Proc. SPIE **8381**, 83811A (2012).
8. J. Swiderski, M. Michalska, and G. Maze, "Mid-IR supercontinuum generation in a ZBLAN fiber pumped by a gain-switched mode-locked Tm-doped fiber laser and amplifier system," Opt. Express **21**, 7851–7857 (2013).
9. J. Swiderski and M. Michalska, "Over three-octave spanning supercontinuum generated in a fluoride fiber pumped by Er & Er:Yb-doped and Tm-doped fiber amplifiers," Opt. Laser Technol. **52**, 75–80 (2013).
10. P. Moselund, C. Petersen, L. Leick, J. S. Dam, P. Tidemand-Lichtenberg, and C. Pedersen, "Highly stable, all-fiber, high power ZBLAN supercontinuum source reaching 4.75 µm used for nanosecond mid-IR spectroscopy," in *Advanced Solid-State Lasers Congress* (Optical Society of America, 2013), p. JTh5A.9.
11. A. M. Heidt, J. H. V. Price, C. Baskiotis, J. S. Feehan, Z. Li, S. U. Alam, and D. J. Richardson, "Mid-infrared ZBLAN fiber supercontinuum source using picosecond diode-pumping at 2μm," Opt. Express **21**, 24281–24287 (2013).
12. J. Swiderski, M. Michalska, C. Kieleck, M. Eichhorn, and G. Maze, "High power supercontinuum generation in fluoride fibers pumped by 2μm pulses," IEEE Photon. Technol. Lett. **26**, 150–153 (2014).
13. R. Thapa, D. Rhonehouse, D. Nguyen, K. Wiersma, C. Smith, J. Zong, and A. Chavez-Pirson, "Mid-IR supercontinuum generation in ultra-low loss, dispersion-zero shifted tellurite glass fiber with extended coverage beyond 4.5μm," Proc. SPIE **8898**, 889808 (2013).
14. V. S. Shiryaev and M. F. Churbanov, "Trends and prospects for development of chalcogenide fibers for mid-infrared transmission," J. Non-Cryst. Solids **377**, 225–230 (2013).
15. R. E. Slusher, G. Lenz, J. Hodelin, J. Sanghera, L. B. Shaw, and I. D. Aggarwal, "Large Raman gain and nonlinear phase shift in high-purity As_2Se_3 chalcogenide fibers," J. Opt. Soc. Am. B **21**, 1146–1155 (2004).
16. E. A. Romanova, Y. S. Kuzyutkina, A. I. Konyukhov, N. Abdel-Moneim, A. B. Seddon, T. M. Benson, S. Guizard, and A. Mouskeftaras, "Nonlinear optical response and heating of chalcogenide glasses upon irradiation by the ultrashort laser pulses," Opt. Eng. **53**, 071812 (2014).
17. J. Hu, C. R. Menyuk, L. B. Shaw, J. S. Sanghera, and I. D. Aggarwal, "Maximizing the bandwidth of supercontinuum generation in As_2Se_3 chalcogenide fibers," Opt. Express **18**, 6722–6739 (2010).
18. R. R. Gattass, L. B. Shaw, V. Q. Nguyen, P. C. Pureza, I. D. Aggarwal, and J. S. Sanghera, "All-fiber chalcogenide-based mid-infrared supercontinuum source," Opt. Fiber Technol. **18**, 345–348 (2012).
19. W. Yuan, "2-10μm mid-infrared supercontinuum generation in As_2Se_3 photonics crystal fiber," Laser Phys. Lett. **10**, 095107 (2013).
20. C. Wei, X. Zhu, R. A. Norwood, F. Song, and N. Peyghambarian, "Numerical investigation on high power mid-infrared supercontinuum fiber lasers pumped at 3 μm," Opt. Express **21**, 29488–29504 (2013).
21. M. Bache, H. Guo, and B. Zhou, "Generating mid-IR octave-spanning supercontinua and few-cycle pulses with solitons in phase-mismatched quadratic nonlinear crystals," Opt. Mater. Express **3**, 1647–1657 (2013).
22. Y. Yu, X. Gai, T. Wang, P. Ma, R. Wang, Z. Yang, D.-Y. Choi, S. Madden, and B. Luther-Davies, "Mid-infrared supercontinuum generation in chalcogenides," Opt. Mater. Express **3**, 1075–1086 (2013).
23. Y. Yu, X. Gai, D.-Y. C. P. Ma, Z. Yang, R. Wang, S. Debbarma, S. J. Madden, and B. Luther-Davies, "A stable broadband quasi continuum mid-infrared supercontinuum generated in chalcogenide glass waveguide," Laser Photon. Rev., to be published (2014).
24. P. Ma, D.-Y. Choi, Y. Yu, X. Gai, Z. Yang, S. Debbarma, S. Madden, and B. Luther-Davies, "Low-loss chalcogenide waveguides for chemical sensing in the mid-infrared," Opt. Express **21**, 29927–29937 (2013).
25. I. Kubat, C. R. Petersen, U. V. Møller, A. Seddon, T. Benson, L. Brilland, D. Méchin, P. M. Moselund, and O. Bang, "Thulium pumped mid-infrared 0.9-9μm supercontinuum generation in concatenated fluoride and chalcogenide glass fibers," Opt. Express **22**, 3959–3967 (2014).
26. C. Agger, C. Petersen, S. Dupont, H. Steffensen, J. K. Lyngsø, C. L. Thomsen, J. Thøgersen, S. R. Keiding, and O. Bang, "Supercontinuum generation in ZBLAN fibers - detailed comparison between measurement and simulation," J. Opt. Soc. Am. B **29**, 635–645 (2012).
27. I. Kubat, C. S. Agger, P. M. Moselund, and O. Bang, "Mid-infrared supercontinuum generation to 4.5μm in uniform and tapered ZBLAN step-index fibers by direct pumping at 1064 or 1550nm," J. Opt. Soc. Am. B **30**,

#213711 - $15.00 USD Received 9 Jun 2014; revised 18 Jul 2014; accepted 19 Jul 2014; published 31 Jul 2014

2743–2757 (2013).
28. I. D. Aggarwal, L. E. Busse, L. B. Shaw, B. Cole, and J. S. Sanghera, Proceedings of the Diode Laser Technology Review, Albuquerque, NM (1998).
29. J. Sanghera and I. Aggarwal, "Active and passive chalcogenide glass optical fibers for IR applications: a review," J. Non-Cryst. Solids **256–257**, 6–16 (1999).
30. Ł. Sójka, Z. Tang, H. Zhu, E. Bereś-Pawlik, D. Furniss, A. B. Seddon, T. M. Benson, and S. Sujecki, "Study of mid-infrared laser action in chalcogenide rare earth doped glass with Dy^{3+}, Pr^{3+} and Tb^{3+}," Opt. Mater. Express **2**, 1632–1640 (2012).
31. Ł. Sójka, Z. Tang, D. Furniss, H. Sakr, A. Oladeji, E. Bereś-Pawlik, H. Dantanarayana, E. Faber, A. B. Seddon, T. M. Benson, and S. Sujecki, "Broadband, mid-infrared emission from Pr^{3+} doped GeAsGaSe chalcogenide fiber, optically clad," Opt. Mater. **36**, 1076–1082 (2014).
32. H. G. Dantanarayana, N. M. Moneim, Z. Tang, L. Sojka, S. Sujecki, D. Furniss, A. B. Seddon, I. Kubat, O. Bang, and T. M. Benson, "Refractive index dispersion of chalcogenide glasses for ultra-high numerical-aperture fiber for mid-infrared supercontinuum generation," Opt. Mater. Express **4**, 1444–1455 (2014).
33. Amorphous Materials Inc., "Chalcogenide glasses," available at http://www.amorphousmaterials.com/products/ (2013).
34. A. Bornstein, N. Croitoru, and E. Marom, "Chalcogenide infrared $As_{2-x}Se_{3+x}$ glass fibers," J. Non-Cryst. Solids **74**, 57–65 (1985).
35. G. E. Snopatin, V. S. Shiryaev, V. G. Plotnichenko, E. M. Dianov, and M. F. Churbanov, "High-purity chalcogenide glasses for fiber optics," Inorg. Mater. **45**, 1439–1460 (2009).
36. M. S. Maklad, R. K. Mohr, R. E. Howard, P. B. Macedo, and C. T. Moynihan, "Multiphonon absorption in As_2S_3-As_2Se_3 glasses," Solid State Commun. **15**, 855–858 (1974).
37. F. Poletti and P. Horak, "Description of ultrashort pulse propagation in multimode optical fibers," J. Opt. Soc. Am. B **25**, 1645–1654 (2008).
38. J. Ramsay, S. Dupont, M. Johansen, L. Rishøj, K. Rottwitt, P. M. Moselund, and S. R. Keiding, "Generation of infrared supercontinuum radiation: spatial mode dispersion and higher-order mode propagation in ZBLAN step-index fibers," Opt. Express **21**, 10764–10771 (2013).
39. S. D. Savage, C. A. Miller, D. Furniss, and A. B. Seddon, "Extrusion of chalcogenide glass preforms and drawing to multimode optical fibers," J. Non-Cryst. Solids **354**, 3418–3427 (2008).
40. T. Nakai, N. Norimatsu, Y. Noda, O. Shinbori, and Y. Mimura, "Changes in refractive index of fluoride glass fibers during fiber fabrication processes," Appl. Phys. Lett. **56**, 203–205 (1990).
41. C. T. Hach, K. Cerqua-Richardson, J. R. Varner, and W. C. LaCourse, "Density and microhardness of As-Se glasses and glass fibers," J. Non-Cryst. Solids **209**, 159–165 (1997).
42. A. M. Heidt, "Pulse preserving flat-top supercontinuum generation in all-normal dispersion photonic crystal fibers," J. Opt. Soc. Am. B **27**, 550–559 (2010).
43. U. Møller and O. Bang, "Intensity noise in normal-pumped picosecond supercontinuum generation, where higher-order raman lines cross into anomalous dispersion regime," Electron. Lett. **49**, 63–65 (2013).
44. B. Ung and M. Skorobogatiy, "Chalcogenide microporous fibers for linear and nonlinear applications in the mid-infrared," Opt. Express **18**, 8647–8659 (2010).
45. G. P. Agrawal, *Nonlinear Fiber Optics*, 4th ed. (Academic, 2007).
46. R. T. White and T. M. Monro, "Cascaded raman shifting of high-peak-power nanosecond pulses in As_2S_3 and As_2Se_3 optical fibers," Opt. Lett. **36**, 2351–2353 (2011).
47. J. Shi, X. Feng, P. Horak, K. Chen, P. S. Teh, S.-U. Alam, W. Loh, D. J. Richardson, and M. Ibsen, "1.06 μm picosecond pulsed, normal dispersion pumping for generating efficient broadband infrared supercontinuum in meter-length single-mode tellurite holey fiber with high Raman gain coefficient," J. Lightwave Technol. **29**, 3461–3469 (2011).
48. D. V. Skryabin, F. Luan, J. C. Knight, and P. St. J. Russell, "Soliton self-frequency shift cancellation in photonic crystal fibers," Science **301**, 1705–1708 (2003).
49. P. Falk, M. H. Frosz, O. Bang, L. Thrane, P. E. Andersen, A. O. Bjarklev, K. P. Hansen, and J. Broeng, "Broadband light generation at 1300 nm through spectrally recoiled solitons and dispersive waves," Opt. Lett. **33**, 621–623 (2008).
50. F. Poletti and P. Horak, "Dynamics of femtosecond supercontinuum generation in multimode fibers," Opt. Express **17**, 6134–6147 (2009).
51. M. Grabka, B. Wajnchold, S. Pustelny, W. Gawlik, K. Skorupski, and P. Mergo, "Experimental and theoretical study of light propagation in suspended-core optical fiber," Acta Phys. Pol. A **118**, 32141–32150 (2010).
52. I. Shavrin, S. Novotny, and H. Ludvigsen, "Mode excitation and supercontinuum generation in a few-mode suspended-core fiber," Opt. Express **21**, 32141–32150 (2013).
53. S. Coen, A. H. L. Chau, R. Leonhardt, J. D. Harvey, J. C. Knight, W. J. Wadsworth, and P. St. J. Russell, "Supercontinuum generation by stimulated raman scattering and parametric four-wave mixing in photonic crystal fibers," J. Opt. Soc. Am. B **19**, 753–764 (2002).
54. C. Moynihan, P. Macedo, M. Maklad, R. Mohr, and R. Howard, "Intrinsic and impurity infrared absorption in As_2Se_3 glass," J. Non-Cryst. Solids **17**, 369–385 (1975).

#213711 - $15.00 USD Received 9 Jun 2014; revised 18 Jul 2014; accepted 19 Jul 2014; published 31 Jul 2014

1. Introduction

Mid-infrared (MIR) supercontinuum (SC) sources have great potential for improving spectral analysis tools, because of their spatial coherence and high power density over a broad bandwidth. A 1-4.5μm SC source was for example used in hyperspectral IR microscopy to demonstrate simultaneous analysis at multiple wavelengths [1]. In the food and pharmaceutical industry, analysis methods, such as fourier transform IR (FTIR) spectroscopy, can be significantly improved by using a broadband high-power SC source [2]. Mid-IR SC sources are also ideal for stand-off detection, where high power density over a broad spectral range is necessary to acquire information about an ensemble of potentially hazardous substances from a safe distance [3]. Some of the current SC lasers yielding the longest IR wavelengths are based on ZBLAN fibres covering the 1-4.75μm spectral range [4–12], and tellurite fibres covering the 1-4.5μm range [13].

To further extend the MIR SC beyond the ZBLAN and tellurite results, materials that offer a broader MIR transmission window are needed. Promising candidates for this are chalcogenide glasses (CHALCS) as these transmit further into the infrared [14] and provide a strong nonlinear material response [15, 16] both of which are crucial in extending the SC. Due to these two features, increasing focus on developing MIR SC sources based on CHALC waveguides and fibres is taking place. Theoretically Hu *et al.* obtained a 2-7μm MIR SC in optimised As-Se microstructure optical fibre (MOF) when pumping at 2.5μm with 1kW peak power (P_0) pulses [17]. Experimentally, Gattas *et al.*obtained a 1.9-4.8μm MIR SC in an As-S fibre. Picosecond long pulses generated from an erbium (Er^{3+}) laser were initially amplified in an erbium/ytterbium (Er^{3+}/Yb^{3+}) amplifier, red shifted and amplified with a thulium (Tm^{3+}) amplifier, and finally red shifted to 2.4μm in a highly nonlinear fibre, where after they were coupled into the As-S fibre for generation of SC [18]. Yuan has numerically shown that an As-Se MOF, having an idealised loss without extrinsic impurities, otherwise typically present in a fabricated fibre, can give a 2-10μm SC when pumped with femtosecond pulses having P_0=10kW at 4.1μm [19]. Wei *et al.* likewise numerically obtained a broadband 2-12μm SC in As_2Se_3 MOF, which was pumped at 2.78μm with P_0=1kW femtosecond pulses from a modelocked Er^{3+}:ZBLAN laser [20]. In just 15mm of bulk $LiInS_2$ material, Bache *et al.* showed numerically that it is possible to obtain a 1-8μm SC when pumping with femtosecond pulses having peak intensities of 300GW/cm^2 launched at 3μm from a tunable Optical Parametric Amplifier (OPA) [21]. Experimentally, Yu *et al.* used an OPA generating femtosecond pulses having P_0=20MW at 5.3μm, where they were able to demonstrate a 2.5-7.5μm SC by pumping a bulk $Ge_{11.5}As_{24}S_{64.5}$ sample [22]. Exchanging the bulk sample with a waveguide having a core composed of $Ge_{11.5}As_{24}Se_{64.5}$ and a cladding of $Ge_{11.5}As_{24}S_{64.5}$ they were able to generate a MIR SC covering the 1.8-7.5μm range when pumping with an OPA at 4μm but now with only P_0=3260W [23]. Similar waveguides have also been successfully utilised in MIR chemical sensing [24]. Likewise, we have also theoretically shown that even a standard, pulsed Tm^{3+} laser operating at 2μm can be used to generate a 0.9-9μm MIR SC in dispersion-optimised CHALC MOF by using a ZBLAN fluoride fibre as an intermediate fibre [25].

In this work simple and robust step-index fibres (SIFs) were considered for the generation of MIR SC, which were based on core/cladding As-Se/Ge-As-Se glasses. In our previous work on designing ZBLAN fluoride SIFs, a single experimentally obtained Sellmeier polynomial was used for the core material together with the assumption of a constant numerical aperture (NA) in order to estimate the dispersion of the cladding material [26, 27]. In contrast, the fibre designs in this work were based on measured bulk material refractive indices for both the core and cladding CHALC materials over the entire wavelength range considered. This is to our knowledge the first design of CHALC SIFs where measured CHALC material refractive indices are utilised for both the core and the cladding leading to a wavelength dependent NA. Furthermore,

#213711 - $15.00 USD Received 9 Jun 2014; revised 18 Jul 2014; accepted 19 Jul 2014; published 31 Jul 2014

we measured the CHALC SIF loss, which in combination with the improved fibre dispersion modeling should make our modeled SC results more accurate in predicting the experimentally obtained MIR SC.

For the formation of MIR SC a MIR laser operating at 4.5μm based on praseodymium (Pr^{3+}) doped CHALC (Pr^{3+}:CHALC) fibres was considered [29–31]. For the laser Gaussian shaped pulses were assumed with a temporal duration (T_{FWHM}, full width at half maximum) of 50ps, and a repetition rate of 4MHz. While some of the previously reported CHALC SC were based on very high peak power [19,21,22], the peak power considered here were at 0.75, 1 and 4.7kW in order to keep the intensities below or at the theoretical peak intensity threshold of 3GW/cm^2 of CHALCs [28, 29]. Furthermore, the pump wavelength of 4.5μm considered and the high NA of the fibres ensured that the material zero dispersion wavelength (λ_{ZDW}) could be reached with either the first, the second, or the third Raman line, which makes the Raman-induced broadening process efficient enough to generate a 3-12.5μm MIR SC.

2. Optical material properties

The glasses and fibres considered here were made at the University of Nottingham, UK. The SIFs had a core made of $As_{40}Se_{60}$ (As-Se) and a cladding made of $Ge_{10}As_{23.4}Se_{66.6}$ (Ge-As-Se). The compositions had sufficient thermal compatibility so that a SIF preform made of the two could be drawn down to a fibre. In order to model the optical properties of the fibres the refractive indices were measured [32] and compared to the As-Se composition AMTIR-2 from Amorphous Materials Inc. [33].

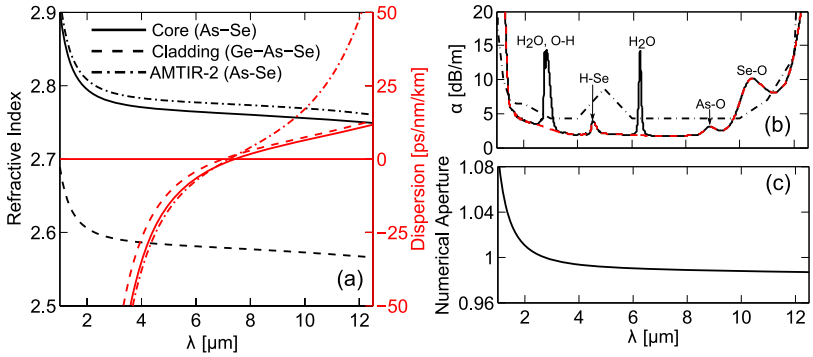

Fig. 1. Optical properties of the CHALC glasses. (a) Refractive index (black) and dispersion (red) of bulk $As_{40}Se_{60}$ (As-Se) (solid), $Ge_{11.5}As_{24}Se_{64.5}$ (Ge-As-Se) (dashed) [32], and AMTIR-2 As-Se (dash-dotted) [33]. (b) Large core (D_c=288μm) fibre loss measurement with different absorption bands indicated (solid black), and an idealised loss without the two strong O-H and H_2O absorption bands at 2.9 and 6.3μm (dashed red) as well as AMTIR-2 As-Se bulk material absorption (dotted black) [33]. (c) NA=$\sqrt{n_{core}^2 - n_{cladding}^2}$ of a SIF with As-Se as core and Ge-As-Se as cladding.

The refractive indices, which were measured using ellipsometry (J.A. Wollam Co., Inc. IR-VASE®) are shown in Fig. 1(a) (black). Comparing the As-Se (solid) core material and the Ge-As-Se (dashed) cladding material with AMTIR-2 (dash-dotted) indicates that the measured As-Se composition was in correspondence with the AMTIR-2, as both have comparable refractive index. The Ge-As-Se glass had a significantly lower index than the other two, allowing it to be used as the cladding of high-NA fibres. The close resemblance between the different bulk glasses can be seen when comparing their material dispersions (red), which were calculated from the refractive indices, with the λ_{ZDW} of core and cladding compositions at 7.4μm and

#213711 - $15.00 USD Received 9 Jun 2014; revised 18 Jul 2014; accepted 19 Jul 2014; published 31 Jul 2014

7.0μm, respectively, and at 7.2μm for the AMTIR-2. For all glasses the dispersion dropped rapidly at wavelengths below their respective λ_{ZDW}s. At wavelengths longer than the λ_{ZDW} a pronounced difference between the glasses is seen as the dispersion of our glasses gradually increased up to 10ps/nm/km at 12μm whereas the dispersion for AMTIR-2 increased up to 50ps/nm/km.

Figure 1(b) shows the fibre loss of a large core SIF having a core diameter (D_c) of 288μm and cladding diameter of 300μm, measured with a FTIR spectrometer in the 1.6-12.5μm range based on the standard cut-back technique [34]. The large core fibre was deliberately chosen in order to couple the low intensity light from the globar in the FTIR into the fiber. The lowest measured loss was 1.68dB/m at 6.97μm and in general a loss below 2.5dB/m was obtainable in the 3.3-9.4μm range. Even lower losses were achieved with further purification [35]. At shorter and longer wavelengths the loss increased sharply. Strong absorption bands at 2.9 and 6.3μm were present due to water impurities (O-H, H_2O). We investigate the influence of these water absorption bands on the developing SC by comparing the modeled spectra obtained with the full loss (solid black curve) and a idealized loss where the two peaks at 2.9um and 6.3um were removed (dashed red curve). For fibres fabricated from the As-Se core and Ge-As-Se cladding glasses the 1.6-12.5μm was considered the effective transmission region of the fibre. Beyond that we extrapolated the loss to 250dB/m at all wavelengths, which was the same as the theoretically estimated loss of the As-Se composition at 16μm by Maklad *et al.* [36].

A comparison of the As-Se/Ge-As-Se fibre loss with that of the AMTIR-2 As-Se bulk glass [33] shown in Fig. 1(b) revealed noticeable differences. The AMTIR-2 had an almost constant loss of 4.34dB/m in the 1-10μm region with a strong peak of 8.7dB/m at 5μm making the AMTIR-2 loss generally higher than the loss of the Nottingham glasses. Some of the current numerical and experimental results on broadband CHALC SC were obtained with a few millimeters or centimeters of waveguide when pumping with very high peak powers [21, 22]. Over such short lengths of waveguide the losses could in practice be neglected. However, such high peak powers are rarely available from lasers outside specialised optical laboratories, so lengths on the order of several centimeters or even meters of fibre need to be considered to obtain the same broadening with lower pump peak powers. Also, in any system of practical interest it is desirable to have a piece of fibre with a reasonable length for fibre handling. Increasing the length of the fibre to accommodate these requirements and the broadening processes will inevitably start to become impaired by loss.

The rate of change in the refractive index with wavelength between the core As-Se and cladding glass Ge-As-Se in Fig. 1(a) was comparable. When calculating the NA=$\sqrt{n_{core}^2 - n_{cladding}^2}$ of a SIF made of the two glasses is shown in Fig. 1(c), which demonstrated a reasonably constant NA around one in the 2-13μm range. The high NA would make sure that the Fundamental Mode (FM) was properly confined to the core at all wavelengths, so the generation of SC could proceed unhindered.

3. Chalcogenide step-index fibre design

Broadband MIR SC sources require a λ_{ZDW} close to the pump wavelength λ_p, a dispersion that is low and anomalous, and a nonlinearity and confinement that is as strong as possible over the entire bandwidth [27]. Furthermore, the fibre should preferably be single mode at λ_p in order to avoid distributing the pump power into higher order modes [37, 38, 50, 52].

For the initial design optimisation SIFs having a core diameter between 5-20μm, and a constant NA between 0.2 and 1.0 were considered. The initial predictions of the optimum NA=1.0 SIFs were finally checked using the measured wavelength dependent NA. Chalcogenide SIFs with lower NAs down to 0.2 were also considered since these had already been fabricated using other compositions such as the ones given by Savage *et al.* [39]. Additionally, glass fibre

#213711 - $15.00 USD Received 9 Jun 2014; revised 18 Jul 2014; accepted 19 Jul 2014; published 31 Jul 2014

properties may differ from those of a well annealed bulk glass sample because the high cooling rate encountered during fibre drawing tends to bestow a higher glass fictive temperature, and so potentially a lower refractive index. This had been observed for fluoride glasses by Nakai *et al.* [40]. Moreover, drawing-induced re-orientation may occur in the case of chain molecular structures which can be present in glasses for instance Se-chains in CHALC glasses [41]. The resulting fibres could thus have a lower NA than the one shown in Fig. 1(c), which can result in noticeable changes in the optical properties of the fabricated fibres. This was thus an additional reason for studying generation of SC in lower NA SIFs.

Figure 2 shows a series of calculated fibre dispersions where the dispersion experienced pronounced changes with changing core size and NA. In Fig. 2(a) NA=0.5 and the core size was

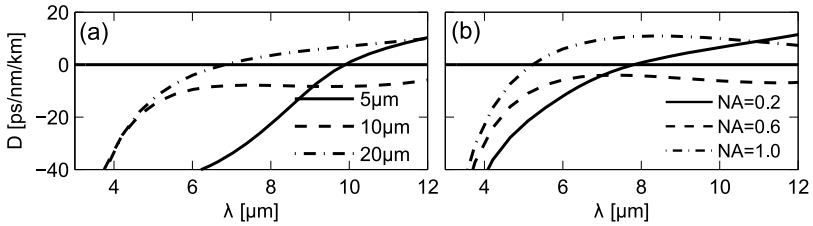

Fig. 2. (a) Dispersion for a SIF with NA=0.5 and core diameter of 5, 10, and 20μm. (b) Dispersion for a SIF with core diameter 10μm and NA of 0.2, 0.6 and 1.0.

varied. The dispersion for the 5μm core diameter SIF (solid) was steep with λ_{ZDW}=10μm. When increasing the core diameter to 10μm (dashed), the dispersion became low and normal from 5 to above 12μm. Such a fibre could be very interesting for all-normal dispersion Self-Phase Modulation (SPM) based coherent SC obtained using femtosecond pump pulses [42]. Here we used picosecond pump pulses to obtain high average power, which meant that the formation of SC was dominated by noise-seeded Raman scattering with no improvement in noise performance similar to anomalously pumped MI-based SC [43]. A further increase in the core diameter to 20μm (dash-dotted) moved the λ_{ZDW} by 4μm to 6.2μm. Additional pronounced changes in fibre dispersion were observed when changing the NA as seen in Fig. 2(b). Here the core diameter was kept at 10μm and the NA was increased from 0.2 to 1.0. The lowest NA=0.2 (solid) dispersion had a λ_{ZDW}=7.9μm and was monotonically increasing. The NA=0.6 fibre (dashed) had a weak all-normal dispersion similar to the NA=0.5 fibre in Fig. 2(a). By increasing the NA to 1.0, the dispersion changed substantially where it became weak and anomalous above λ_{ZDW} at 5.2μm.

Due to these quite pronounced changes in fibre dispersion, a more extended analysis of the optical properties was conducted as shown in Fig. 3. In Fig. 3(a) we see the fibre loss edge defined as the wavelength where the calculated fibre confinement loss reached a loss of 3dB/m [27]. For the smallest core of 5μm with a low NA=0.2, the λ_{3dB} was below 4μm, meaning that the design would not be able to guide even the pump at 4.5μm. Increasing the core diameter moved the λ_{3dB} above 8μm. Increasing NA gradually moved λ_{3dB} for all core geometries to longer wavelengths and for NA$\geq$ 0.6 even the smallest core of 5μm was guiding light beyond 10μm.

The pump at λ_p=4.5μm was in the normal dispersion regime for all of the different designs considered, as seen in Fig. 3(b). Starting with the 20μm core the dispersion was around -20ps/nm/km for all the different NAs. The normal dispersion for the SIFs with NA=1.0 and 0.8 became weaker as the core diameter was decreased, until reaching a minimum value and then rapidly increasing again. For NA=1.0 the minimum normal dispersion was close to zero, indicating that the λ_{ZDW} approached λ_p. For SIFs with NA at 0.6 and 0.4 the dispersion remained

#213711 - $15.00 USD Received 9 Jun 2014; revised 18 Jul 2014; accepted 19 Jul 2014; published 31 Jul 2014

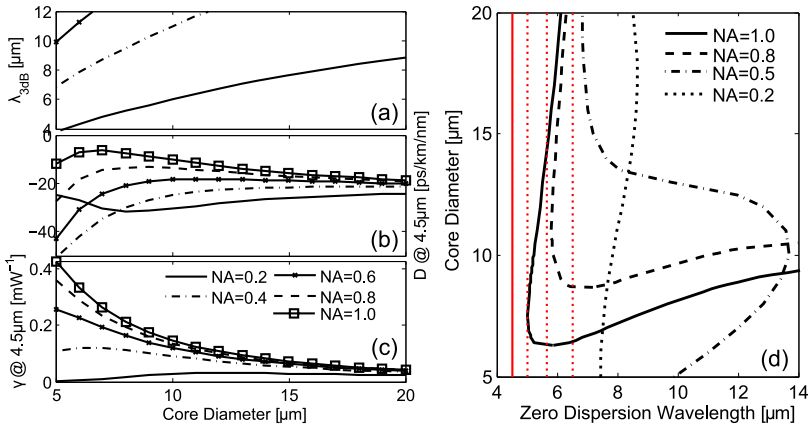

Fig. 3. Detailed analysis of fibre optical properties. (a) Fibre confinement loss edge λ_{3dB}, (b) dispersion D at λ_p=4.5μm, and (c) nonlinearity γ at λ_p vs. core diameter for different NA. (d) Zero Dispersion Wavelengths for different core diameter and NA. The solid red line indicates the pump at 4.5μm and dotted red lines are the first three Raman Stokes lines based on the model by Ung *et al.* [44].

constant around -20ps/nm/km for the larger core diameters where after it became stronger for core diameters below 10 and 12μm, respectively. For the fibre with NA=0.2, the dispersion decreased as the core size was decreased, but started to increase again for core size below 7μm.

The nonlinearity, given as $\gamma = 2\pi n_2/(A_{eff}(\lambda)\lambda)$ with $n_2 = 5.2 \cdot 10^{-18}$ m^2/W at 4.5μm [15, 16] and $A_{eff}(\lambda) = (\int\int |\mathbf{E}(\lambda)|^2 dxdy)^2 / \int\int |\mathbf{E}(\lambda)|^4 dxdy$ [45], was evaluated at λ_p and is shown in Fig. 3(c). It increased with decreasing core size and increasing NA as expected, since both would decrease $A_{eff}(\lambda)$ of the mode. This is the case for all the NAs but the two lowest, which could not confine the mode properly at 4.5μm. The nonlinearity for the smaller cores and the lowest NAs of 0.2 and 0.4 decreased, which was due to poor mode confinement. This corresponded well with the low mode confinement seen in the short λ_{3dB} for the same NAs in Fig. 3(a).

A detailed summary of λ_{ZDW} is shown for core diameters in the 5-20μm range and NA=0.2, 0.5, 0.8, and 1.0 in Fig. 3(d). The solid red line is the pump at 4.5μm and the dotted red lines are the first three Raman Stokes lines calculated from the measured As-Se Raman response reported by Ung *et al.* [44]. For all the fibres considered there was a spectral gap between λ_p and the first λ_{ZDW}. Given that the pump considered had long picosecond pulses it would be the strong Raman scattering generating a cascade of Raman stokes similar to that reported by White *et al.* [46] that would be responsible for pushing light above the λ_{ZDW}, similar to the example experiments by Shi *et al.* in tellurite fibres [47] and Møller *et al.* in silica fibres [43].

For NA=0.2 the λ_{ZDW} was around 7.5-8.5μm. Increasing the NA to 0.5 made the changes in λ_{ZDW} more sensitive to changes in the core diameters. In particular the λ_{ZDW} now came closer to the third Raman line for the core diameters over 15μm. For a core diameter of 10μm the λ_{ZDW} shifted to 13.5μm, which in fact provided a low and normal dispersion from 5 to 13.5μm as seen in Fig. 2(b). Increasing NA moved the λ_{ZDW} to shorter wavelengths as seen for NAs 0.8 and 1.0, where the λ_{ZDW} was shifted down to 5μm for core diameter of 8μm and NA=1.0. For the two highest NAs an additional λ_{ZDW} appeared for the smallest core diameters. These type of changes in soft glass fibre dispersion seem to be generic when changing their core size and NA, as we reported similar trends for ZBLAN SIFs for MIR SC in the 1-5μm region [27].

The NA=1.0 and 8μm core fibre has the best confinement, the strongest nonlinearity, the

#213711 - $15.00 USD Received 9 Jun 2014; revised 18 Jul 2014; accepted 19 Jul 2014; published 31 Jul 2014

lowest dispersion at the pump, and the shortest λ_{ZDW}. The fibre therefore seemed as the obvious choice for efficient generation of broadband MIR SC. However, the fibre had a second λ_{ZDW} at 9.7μm, which would stop the soliton based spectral broadening due to spectral recoil [48]. With this in mind the SIF with a core diameter of 10μm and NA=1.0 could be a more suitable choice as it did not have a second λ_{ZDW}, thereby allowing the spectral broadening to proceed to the long wavelength transmission edge of the CHALC fibre. In the 8μm core and NA=1.0 fibre the long wavelength edge of the developed SC, the IR edge, will be comprised of Dispersive Waves (DWs) due to the second λ_{ZDW} whereas in the 10μm and NA=1.0 fibre it would consist of solitons. This would result in two different SC spectra, which are tested in the following. Similar investigation has been conducted for near-IR SC in silica PCFs showing an almost equal efficiency of generation [49].

For larger core diameters of 20μm or above, both the nonlinearity and the λ_{ZDW} of the NA=0.5-1.0 fibres approached each other, as seen in Figs. 3(c)–3(d), respectively. The only difference was that the λ_{ZDW} of the NA=0.5 fibre moved just above the 3rd Raman line. With the aim scaling up the SC power the performance of the 20μm NA=0.5 and 0.8 fibres was therefore considered in the following.

4. Small core and large nonlinearity fibre for mid-infrared supercontinuum generation

First, MIR SCG was investigated in CHALC SIFs having the wavelength dependent NA=1.0, and the smallest core diameters of 8 and 10μm. These core geometries *c.f.* Fig. 3 offer the shortest λ_{ZDW} and highest nonlinearities, hence these should be the ones that lead to most efficient formation of broadband SC. The pump pulses were 50ps and had peak power of 0.75 and 1kW for the two cores respectively, in order to stay at or below the previously mentioned theoretical damage threshold of 3GW/cm^2 [28, 29].

The pulse propagation in CHALC fibres was modeled using the Generalised Nonlinear Schrödinger Equation (GNLSE) for single mode and single-polarisation, as detailed in [26, 27] for fluoride fibres. For the nonlinear material response a wavelength depended Kerr coefficient n(λ) found in [16] was used together with the Raman profile taken from [44]. The high NA of the fibres allowed them to guide multiple modes with around 20 guided modes at 4.5μm for the D_c=10μm and NA=1.0 fiber, which had a V-number around 7, so some of the pump power could be lost to higher order modes. However, proper incoupling can ensure excitation of the FM only, which would be responsible for the majority of the broadening [49-51]. Since the fibres considered were not polarisation maintaining, during propagation the power would be distributed between the two polarisations of FM due to Cross-Phase Modulation (XPM) [53], which would effectively reduce the available peak power by a factor of two thereby limiting the potential broadening. However, the model was still be able to point out the optimum fibre design for efficient generation of broadband MIR SC.

Formation of SC in fibres having the wavelength dependent NA of 1.0 is given in Fig. 4. Generation of MIR SC in the first fibre with the 8μm core is seen in Fig. 4(a), which had two λ_{ZDW}s at 5.1 and 9.43μm (solid black), and a dispersion and nonlinearity at λ_p of -7.35ps/nm/km and 0.2 m^{-1}W^{-1}, respectively. The contour plot shows how the SC developed over 2m of fibre. As the pump pulse propagated down the fibre it generated a cascade of Raman Stokes lines, which in turn generated a cascade of Raman anti-Stokes lines through non-phase matched parametric amplification [53]. The Raman induced broadening was gradually exchanged with soliton based broadening, which in turn generated DWs accross the second λ_{ZDW} where the full broadening developed over 1m of fibre. The final spectra of the developed SC with the full (black) and reduced (red) loss profiles indicated no noticeable difference, so for this SIF and pump specifications the O-H and H_2O absorption bands at 2.9 and 6.3μm (see Fig. 1(c)) did not seem to pose any significant hindrance for the developing of SC.

#213711 - $15.00 USD Received 9 Jun 2014; revised 18 Jul 2014; accepted 19 Jul 2014; published 31 Jul 2014

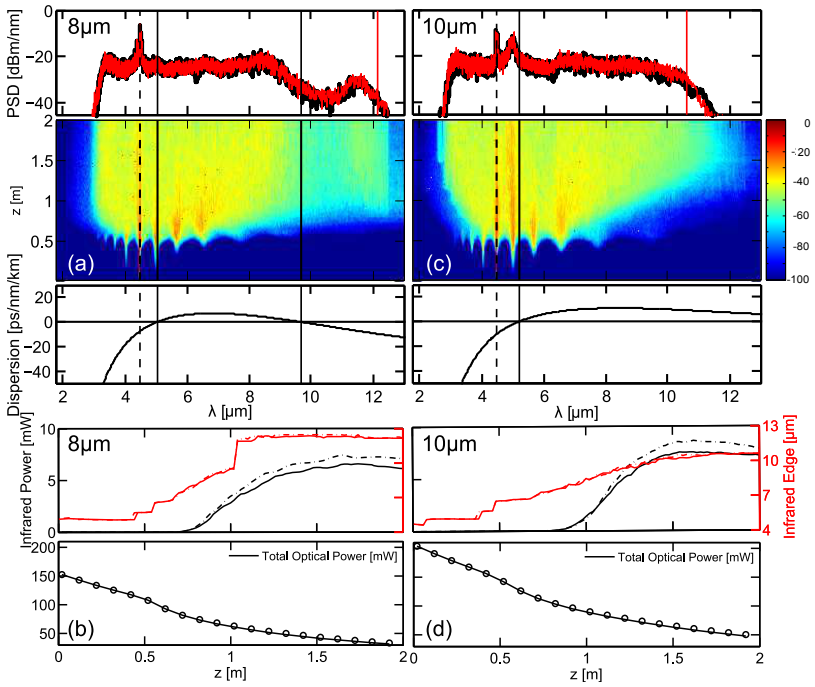

Fig. 4. Ensemble averaged (five seed) MIR SC generated in CHALC SIFs with wavelength dependent NA of 1.0. (a) Generation of SC in the 8μm fibre. Top: SC output spectra for the full (black) and reduced (red) fibre loss profile at the end of the fibre. Middle: Contour plot of the SC as it developed over 2m. Bottom: Fibre dispersion. The λ_p, λ_{ZDW}, and -20dB IR edge are given as dashed black, solid black, and solid red vertical lines, respectively. (b) The IR power (8-10μm band) (black) and IR edge (red) with the full (solid) and reduced (dashed-dotted) fibre loss profiles. Below is the total optical power for the full (solid) and reduced (circles) loss profiles. (c-d) Generated MIR SC in the D_c=10μm fibre with the same notation.

Figure 4(b) shows how the SC developed in terms of the accumulated IR power in the 8-10μm range (black) and the -20dB IR edge (red) with the full (solid) and reduced (dashed) fibre loss. It is seen how onset of broadening began around 50cm of propagation and continually extended the spectrum out to the long wavelength transmission edge of the fibre of 12.5μm, which was initially due to Raman scattering followed by soliton self-frequency shifting. The accumulated IR power, in the 8-10μm range, peaked at approximately 1.7m with around 6.6 and 7.5mW converted power for the full and reduced fibre losses, respectively. Unlike the IR edge the converted IR power was affected by the prominent water bands. The total optical power seen below in the figure for both the full (solid) and reduced (circle) fibre losses decreased from around 150 to around 30mW with slight increase in the loss with the onset of broadening. In terms of total power there were no noticeable difference in the loss between the full and reduced loss profiles.

Figure 4(c) shows how the MIR SC was generated in the D_c=10μm fibre. This fibre had a single λ_{ZDW} at 5.2μm and the dispersion and nonlinearity at λ_p of -10.2ps/nm/km and 0.15 $m^{-1}W^{-1}$, respectively. With the slightly longer λ_{ZDW} and lower nonlinearity, 2m of fibre was needed to obtain the full broadening, and for this fibre the SC extended out to 10.7μm, which was the wavelength region where the fibre loss increased locally due to Se-O impurities [54] and intrinsic material losses [36] as seen in Fig. 1(b). The contour plots of the developing of SC

#213711 - $15.00 USD Received 9 Jun 2014; revised 18 Jul 2014; accepted 19 Jul 2014; published 31 Jul 2014

shows that as in the 8μm fibre there was no noticeable broadening the first 50cm followed by a gradual broadening out to 10.7μm over the remainder of the 2m fibre. Comparing the developed SC with the full and reduced fibre loss profiles given as black and red spectra, respectively, seen in Fig. 4(d), again did not reveal any noticeable changes in terms of the development of the SC due to the two strong water absorption bands as in the 8μm fibre.

The evolution of the IR power and edge of the developing SC in Fig. 4(d) shows that the maximum power conversion into the 8-10μm band was 7.6 and 8.6mW for the full and reduced fibre losses, respectively, and was obtained in around 1.6m of fibre. This was slightly shorter than the 1.64m necessary in the 8μm fibre for the maximum power conversion, which is due to higher peak power utilised. Just as in the 8μm core fibre the loss bands at 2.9 and 6.3μm lead to small deviation in converted power due to the loss bands at 2.9 and 6.3μm.

Comparing the SC spectrum of the two fibres as seen in Figs. 4(a)–4(c) shows a more uniform SC spectrum being obtained in the 10μm fibre out to 10μm with the absence of the second λ_{ZDW}. This was because the solitons in the 8μm fibre experienced cancellation of soliton self-frequency shift due to spectral recoil and formation of DWs across the second λ_{ZDW} [48, 49], which depleted their energy and the whole SC around the second λ_{ZDW}. Apart from the difference in shape of the SC spectrum the two different pump and fibre configurations yielded almost the same IR powers.

5. Large core and high average power fibre for mid-infrared supercontinuum generation

For applications such as stand-off detection and IR counter measures, not only a broad bandwidth but also a high average power in the MIR spectral range is required. In order to accommodate this, large core fibres are needed, as increasing the core size increases the power handling ability of the fibres. Increasing the average power of the MIR SC was done by increasing the average power of the pulsed pump source given as P_{avg}=1.06$P_0 T_{FWHM} \nu_r$ for a Gaussian pulse. With ν_r =4MHz and T_{FWHM}=50ps pulses with an increased peak power of 4.7kW were considered that yielded an average pump power of around 1W. Apart from the increased average power the increased peak power was crucial in overcoming the much lower nonlinearity of the larger core fibres.

The fibres considered had a core size of 20μm and NA=$\{0.5, 0.8, 1.0\}$. As seen in Fig. 3, scaling up the core size and reducing the NA shifted the λ_{ZDW} to longer wavelengths and decreased the nonlinearity. Both changes in fibre dispersion and nonlinearity impaired the fibre in broadening the SC spectrum out to the long wavelength transmission edge of the fibre.

Figure 5 shows generated MIR SC in the 20μm fibres that had a wavelength dependent NA of 1.0. Figure 5(a) shows the generated MIR SC at the end of 2m of fibre, pumped with the 1kW peak power pulse used previously to study the small core fibre designs. The fibre had a λ_{ZDW}=6.11μm, and dispersion and nonlinearity at λ_p of -19ps/nm/km and 0.04$m^{-1}W^{-1}$, respectively. The SC spectrum for both the full (black) and reduced (red) fibre loss profiles extended to 7μm, which was due to a single Raman line building up followed by its own SPM broadening. Figure 5(b) shows a completely unchanged IR edge (red) and an IR power (black) at zero, which shows that the 1kW peak power pump was not able to generate any noticeable broadening in this large core fibre. The evaluated total power shown below in Fig. 5(b) for both full (solid) and reduced (circles) fibre loss profiles continually decreased over the entire length of fibre from 200 down 45mW. A longer length of fibre would not yield any more broadening as any formation of higher order Raman lines would decrease in power due to the fibre losses thereby effectively stopping the broadening processes.

Figure 5(c) shows the generated SC the same fibre but with 4.7kW peak power pulses, which were still below the theoretical damage threshold. In this case a broadening out to 10.6μm was obtained over 2m of fibre. Compared to the small core fibres the increased peak power resulted

#213711 - $15.00 USD Received 9 Jun 2014; revised 18 Jul 2014; accepted 19 Jul 2014; published 31 Jul 2014

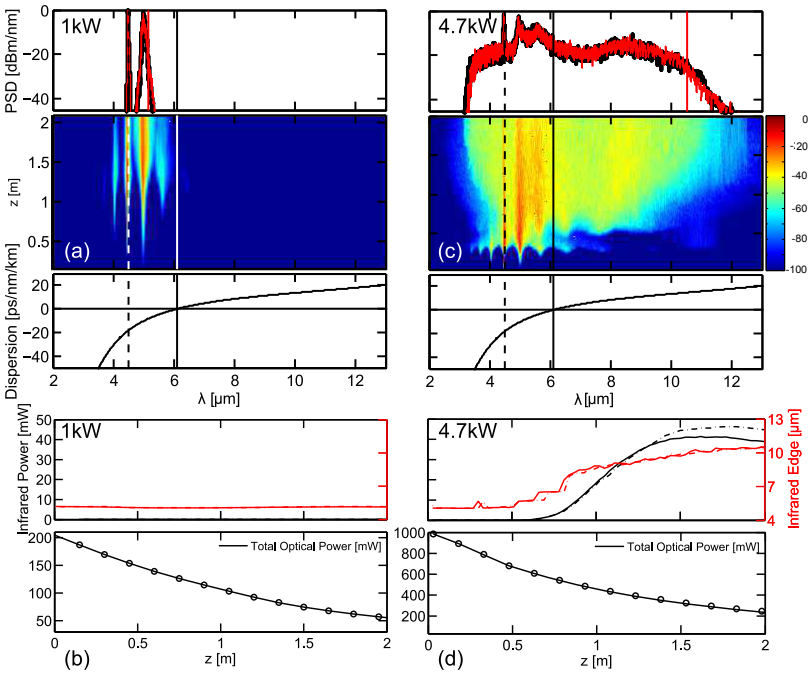

Fig. 5. Ensemble averaged (five seed) MIR SC in CHALC SIFs with D_c=20μm and wavelength depended NA around one. (a) The generated SC when using P_0=1kW and L=2m. Top: Output SC spectrum for the full (black) and reduced (red) loss profile. Middle: Contour plot of the SC as it developed over 2m. Bottom: Fibre dispersion. The λ_p, λ_{ZDW}, and -20dB IR edge are given as dashed black, solid black, and solid red lines, respectively. (b) The IR power (8-10μm band) (black) and IR edge (red) with full (solid) and reduced (dash-dotted) loss profile. At the bottom is given the total optical power for the full (solid) and reduced (circles) loss profiles. (c-d) Generated MIR SC in the same fibre with a length of 2m and P_0=4.7kW.

also in an increased power spectral density over the entire SC. The evaluated IR edge of the SC in Fig. 5(d) shows how it extended out to 10.6μm where it too stopped due to the intrinsic and extrinsic fibre losses [36, 54] just like the 10μm fibre. Due to the larger average power, the maximum converted IR powers were 41 and 46mW for the full and reduced fibre losses, respectively, and were in 1.6 and 1.8m of fibres. The total power in Fig. 5(d) was continuously decreasing from around 996 to 200mW. The total output power was still higher than the output power when utilising the smaller core fibres. Employing larger fibre cores thus allowed for utilisation of high peak powers pulses, which lead to a higher spectral power density as well as a higher IR power.

Formation of MIR SC in the 20μm core lower NA fibres of 0.8 and 0.5 is shown in Fig. 6. The MIR SC at the end of the NA=0.8 SIF fibre is seen in Fig. 6(a) where a pulse with P_0=4.7kW was propagated over 2.25m. The fibre had the λ_{ZDW}=6.28μm while the dispersion and nonlinearity at λ_p were at -19.2ps/nm/km and 0.04m^{-1}W^{-1}, respectively. For both the full and reduced fibre loss profiles the spectrum extended out to 10.3 and 10.4μm, respectively.

The IR power and IR edge of the developing SC is seen in Fig. 6(b). The IR edge indicated that the broadening began to stagnate at the end of the 2.25m of fibre, which was comparable to the NA=1.0 fibre (see Fig. 5(d)). The highest IR power was 38mW in 1.9 and 42mW in 2m of fibre for the full and reduced losses, respectively, and it required slightly longer length of fibre

#213711 - $15.00 USD Received 9 Jun 2014; revised 18 Jul 2014; accepted 19 Jul 2014; published 31 Jul 2014

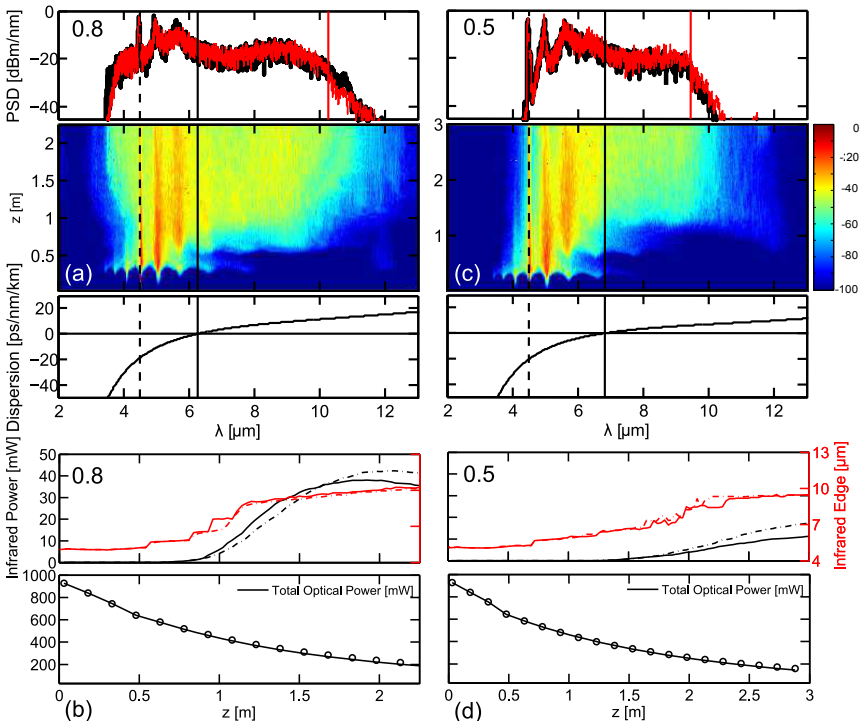

Fig. 6. Ensemble averaged (five seed) MIR SC in CHALC SIFs with D_c=20μm with NA={0.5,0.8} and P_0=4.7kW. (a) The SC spectrum in the fibre with NA=0.8 and the fibre length of L=2.25m. Middle: Contour plot of the SC as it developed over 2.25m. Top: Output SC spectrum for the full (black) and reduced (red) loss profile. Bottom: Fibre dispersion. The λ_p, λ_{ZDW}, and -20dB IR edge as dashed black, solid black, and solid red lines, respectively. (b) IR power (8-10μm band) (black) and IR edge (red) with the full (solid) and reduced (dash-dotted) loss profile. At the bottom is given the total optical power for the full (solid) and reduced (circles) loss profiles. (c-d) Generated MIR SC in the NA=0.5 fibre with length L=3m.

due to the lower nonlinearity and longer λ_{ZDW}. The change in total power of the NA=0.8 fibre was comparable to the NA=1.0 when pumping with the same pulses, as 2.25m of fibre reduces the power from 996 to 200mW.

The generated MIR SC at the end of 3m of the NA=0.5 fibre is seen in Fig. 6(c). The fibre had a λ_{ZDW}=6.8μm, and a dispersion at λ_p of -20.7ps/nm/km and nonlinearity at λ_p of 0.04m^{-1}W^{-1}, which was the lowest of the fibres considered. The SC extended to around 9.5μm where the SC IR edge stopped for both the full and reduced fibre loss profiles. Evaluating the IR power and IR edge was done in Fig. 6(d). Both the largest broadening and the highest power conversion was obtained over three meter of fibres due to the much lower nonlinearity than the NA=0.8 and NA=1.0 fibres. The obtained IR powers were 11mW and 17mW for the full and reduced fibre losses, respectively, which was the largest deviation between the full and reduced loss of the fibres considered. Just like the previous two fibres the total power decreased continually from around 996 to 200mW.

#213711 - $15.00 USD Received 9 Jun 2014; revised 18 Jul 2014; accepted 19 Jul 2014; published 31 Jul 2014

6. Conclusions

We have presented a detailed study of 4.5μm pumped MIR SC generation in CHALC SIFs based on measured material dispersion and fibre loss data covering the 1.6-12.5μm wavelength region. The considered fibres were made from a unique thermally compatible As-Se and Ge-As-Se glass pair promising ultra-high NA's around one. The pump source was proposed to be a Pr^{3+}:CHALC fibre laser with a repetition rate of 4MHz, giving 50ps pulses with a peak power of 4.7kW, in order to satisfy the physical limit on the applicable peak power imposed by the CHALC material [28, 29].

Fibre design studies revealed two interesting regimes. The NA=1.0 fibres were demonstrated always to be the optimum compared to lower NA fibres, with a lowest possible λ_{ZDW} of 5μm being obtained for a core diameter of 8μm. Due to the presence of a second λ_{ZDW} at 9.43μm for the 8μm fibre it was shown that the NA=1.0 fibre with a 10μm core diameter seemed to be the optimum in terms of generating a flat SC spectrum because it had no second λ_{ZDW}. However, the 8μm core was the only design that was able to extend the spectrum out the long wavelengths transmission edge of the fibres at 12.5μm. This was because the second λ_{ZDW} allowed for formation of MIR DWs that were able to push the light further past the point where soliton self-frequency shifting stopped extending the spectrum in the 10μm fibre at 10.7μm. For both fibres Raman scattering was necessary for the spectrum to cross λ_{ZDW} as the pump was located in the normal dispersion regime. Both for the 8 and 10μm core two Raman lines were necessary to cross λ_{ZDW}, although the first Raman line was very close to λ_{ZDW} for the 8μm core fiber. The fibres were able to convert 7.5 and 8.6mW, respectively, into the 8-10μm band. The broadest bandwidth obtained was from 3 to 12.5μm in the 8μm fibre.

The second interesting fibre design regime was for core diameters of 20μm or above, for which the nonlinearity and λ_{ZDW} of the fibres with NA between 0.5 and 1.0 approached each other. The λ_{ZDW} was then below the third Raman Stokes line for the NA=1.0 and 0.8 fibres, but just above for the NA=0.5 fibre. This could potentially provide a convenient design freedom in terms of the NA and the larger core could improve the power handling capabilities of the fibre. Due to the lower nonlinearity of the large core fibres an increased peak power of 4.7kW was considered in order to push the spectrum into the mid-IR, which was comparable to the theoretical damage intensity threshold of 3GW/cm^2 [28, 29]. The NA=1.0 and 20μm core diameter fibre were demonstrated to be able to generate a 3-10.6μm SC with around 46mW in the 8-10μm region. The NA=0.8 fibre was demonstrated to have similar performance, while the NA=0.5 fibre did not perform nearly as efficient as it needed four Raman Stokes lines to cross the λ_{ZDW}.

Acknowledgments

We thank Prof. V Shiryaev of the Russian Academy of Science, Institute for High Purity Chemicals, Russia, for helpful discussion on loss in the 10-20 micron wavelength region. This research has been supported by the European Commission through the Framework Seven (FP7) project MINERVA (317803; www.minerva-project.eu).

#213711 - $15.00 USD Received 9 Jun 2014; revised 18 Jul 2014; accepted 19 Jul 2014; published 31 Jul 2014